Int J Earth Sci (Geol Rundsch) (2016) 105:1015–1020
DOI 10.1007/s00531-015-1206-y

ORIGINAL PAPER

Kinematics and shear heat pattern of ductile simple shear zones with 'slip boundary condition'

Kieran F. Mulchrone[1] · **Soumyajit Mukherjee**[2]

Received: 15 February 2015 / Accepted: 25 May 2015 / Published online: 5 June 2015

Abstract Extrusion by Poiseuille flow and simple shear of hot lower crust has been deciphered from large hot orogens, and partial-slip boundary condition has been encountered in analogue models. Shear heat and velocity profiles are deduced from a simplified form of Navier–Stokes equation for simple shear together with extrusive Poiseuille flow and slip boundary condition for Newtonian viscous rheology. A higher velocity at the upper boundary of the shear zone promotes higher slip velocity at the lower boundary. The other parameters that affect the slip are viscosity and thickness of the shear zone and the resultant pressure gradient that drives extrusion. In the partial-slip case, depending on flow parameters (resultant pressure gradient, density and viscosity) and thickness of the shear zone, the velocity profiles can curve and indicate opposite shear senses. The corresponding shear heat profiles can indicate temperature maximum inside shear zones near either boundaries of the shear zone, or equidistant from them.

Keywords Simple shear · Slip boundary condition · Velocity profile · Viscous dissipation

Introduction

The study of ductile shear zones is of great importance in tectonics and earthquake studies (Regenauer-lieb and Yuen 2003). Simple shear, a type of ductile shear, involves movement of boundaries parallel to themselves (Ramsay 1980). This leads to movement of material points within the shear zone parallel to the shear zone boundaries. This deformation has been well described in fluid mechanics as Couette flow (Schlichting and Gersten 1999) where a linear velocity profile forms when the boundaries are parallel. A second classical consideration in structural geology has been that the 'no-slip boundary condition' prevails during all kinds of shear deformation. This means that the fluid in contact with the solid boundary is presumed to attain the same velocity as the boundary. The theory of Prandtl layer suggests this no-slip boundary condition (Eckert 2006).

In two aspects, the concept needs revision: (1) 'slip boundary conditions' may prevail in shear zones in rocks; and (2) simple shear in large hot orogens, such as in the Greater Himalayan Crystallines (GHC) in the Himalaya (Beaumont et al. 2001) and Andes (Rivers 2009), is accompanied by an extrusive pressure gradient-induced Poiseuille flow where slip boundary condition is to be applied. High-strain zones would develop near the shear zone boundaries in the case of slip boundary condition, and this is similar to the no-slip condition. Conventional shear strain analyses (Davis et al. 2012; Mukherjee 2015 etc.) therefore may not discriminate ductile shear zones with from without slip boundary conditions. Whether or not 'no-slip' or slip boundary conditions occur in geological shear zones has not been tested or discussed explicitly (e.g. in Fleitout and Froideavaux 1980; Ramsay 1980; Regenauer-Lieb and Yuen 2003). However, Czeck and Hudleston (2004) reviewed possibility of slip boundary conditions in transpression zones. Typically, ductile shear fabrics (Berthé et al. 1979; Mukherjee 2011), usually devoid of markers, are inconclusive. Note that Duprat-Oualid et al. (2015) recently presented diffusion, advection and shear

✉ Soumyajit Mukherjee
soumyajitm@gmail.com

[1] Department of Applied Mathematics, School of Mathematical Sciences, University College, Cork, Ireland

[2] Department of Earth Sciences, Indian Institute of Technology Bombay, Powai, Mumbai 400 076, Maharashtra, India

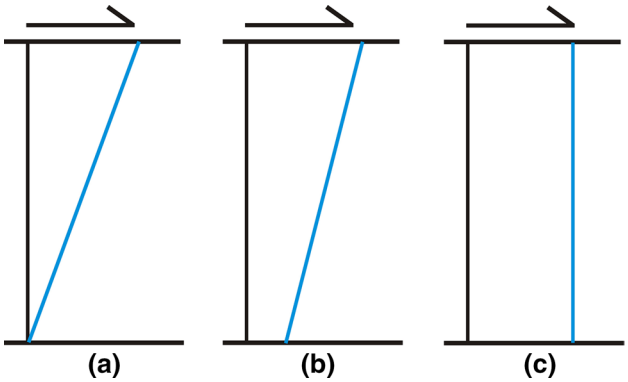

Fig. 1 Couette flow with three possibilities of slip. *Blue lines* velocity profiles. Drawn following Fig. 19.1 of Lauga et al. (2007). **a** No slip $\lambda = 0$, **b** partial slip $0 < \lambda \infty$, **c** perfect slip $\lambda = \infty$

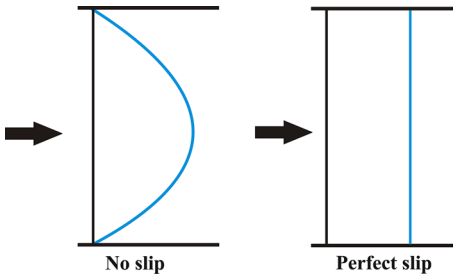

Fig. 2 Poiseuille flow with no slip and perfect slip. *Blue lines* velocity profiles. Drawn following Fig. 1 of Richardson (1973)

heat though a numerical model as the three sources of heat in ductile shear zones. These authors considered all these three components to be important and did not undermine shear heat.

Lauga et al. (2007) pictorially presented 'slip length' (λ) that quantifies 'no slip' ($\lambda = 0$), 'partial slip' ($\infty > \lambda > 0$) and 'perfect slip' ($\lambda = \infty$) (Fig. 1). Richardson (1973) presented an easy-to-comprehend diagram of channel/Poiseuille flow with no slip ($\lambda = 0$) and with complete slip ($\lambda = \infty$) (Fig. 2). It is worth noting that in Fig. 2, perfect slip is applied to both the upper and lower boundaries in contrast to the model presented below. A slip boundary condition is applied at a single boundary for the sake of simplicity. Recent fluid mechanics texts refer/review that slip boundary condition is not uncommon in nature (Boquet and Barrat 2007; Lauga et al. 2007). Melts of polymers at elevated pressure flow with a slip boundary condition (Pozrikidis 2009). λ rises with viscosity, rate of shear and wetting. Also, the less hydrophobic the shear zone boundary is, the higher the value of λ (Bonaccurso et al. 2003). Ductile deformation of rock is approximated by a linear viscous fluid.

Shear zones associated with rifts formed in the lower crust and upper mantle can be hydrated significantly, and simple shear can be the dominant deformation mechanism (Muntener and Hermann 2001). Shear zones in ridge tectonics allows fluid infiltration (Boudier and Al-Rajhi 2014) and subsequent additional lubrication. That melt influx/partial melting can augment ductile shear is well known (Hollister and Crawford 1986). Such melt-triggered shear happens usually in low-grade rocks (Passchier and Trouw 2005). Presence of leucogranitic melt along both S- and C-shear planes observed in migmatites in meso-scale has been interpreted as syn-shear migmatization (Mukherjee 2007, 2010, 2014a; Mukherjee and Koyi 2010). Melts in ductile shear zones might lubricate and create a slip boundary condition.

The GHC, recognised as a ductile shear zone (Mukherjee and Koyi 2010), dips ~N/NE at 30°–60° (Mukherjee 2013), and there was an influx of fluid into the GHC across its lower and southern boundary: the Main Central Thrust (MCT) (Guo and Wilson 2012). This suggests that slipping might occur along the southern boundary of the GHC during the evolution of the shear zone whatever be the fluid influx mechanism. It is not possible to quantify λ at the southern boundary.

Simple shear experiments performed in geological laboratories have created partial-slip conditions despite aiming for 'no-slip' conditions (Frehner et al. 2011). Mukherjee et al. (2012) documented Poiseuille flow with slip in their analogue-modelled slow extrusive flow of Newtonian viscous polydimethylsiloxane through an inclined channel. Velocity profiles for (1) plane Poiseuille flow with slip and no-slip conditions, (2a) Poiseuille flow through inclined channel and (2b) Couette–Poiseuille flow are already available (Papanstasiou et al. 2000; see Warren et al. 2008a, b, c for geological/tectonic contexts). Shear heat profiles for a single- layered and double-layered simple shear zones under no-slip boundary condition too were deduced (Mukherjee and Mulchrone 2013; Mulchrone and Mukherjee in press). This paper deduces velocity and shear heat profiles for ductile simple shear zones with an extrusive Poiseuille flow component and a slip boundary condition.

The model

Velocity profiles

A shear zone inclined at an angle θ to the horizontal is considered with thickness h (Fig. 3). The shear zone comprises a Newtonian viscous fluid of density ρ_c and viscosity μ. A pressure gradient of $\mathrm{d}p/\mathrm{d}x$ acts along the channel which is related to a gravity component acting on the material inside shear zone ($\rho_c g \sin\theta$) and an extrusion component (E) which may be due to a number of factors including density driven extrusion or possibly orogenic collapse. A velocity of U in the positive x direction is present at the upper

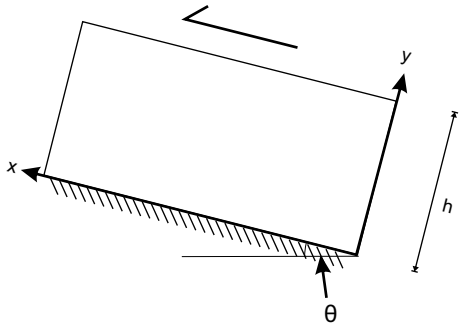

Fig. 3 Layout of the inclined channel considered in model in 'The model' section

boundary (Fig. 3), and slip occurs at the lower boundary. Slip is modelled by a Navier boundary condition (Boquet and Barrat 2007) whereby the shear stress at the slipping interface is proportional to the difference in velocity across the boundary with constant of proportionality κ. In this model, $\lambda = \frac{\mu}{\kappa}$.

The governing equation for velocity u in the x direction is (Turcotte and Schubert 2002, pp. 227–228):

$$\mu \frac{\mathrm{d}^2 u}{\mathrm{d}y^2} = \frac{\mathrm{d}p}{\mathrm{d}x} \tag{1}$$

where in the present case: $G = E - \rho_c g \sin\theta$; $\mathrm{d}p/\mathrm{d}x = -G$.

In other words when $E > \rho_c g \sin\theta$, then $G > 0$ and the Poiseuille component of the flow is up the channel. Relevant boundary conditions are:

$$u(h) = U; \quad u(0) = \frac{\mu}{\kappa}\left(\frac{\mathrm{d}u}{\mathrm{d}y}\right)_{y=0}$$

Noting that $\tau = \mu \frac{\mathrm{d}u}{\mathrm{d}y}$ is the shear stress, κ in the second boundary condition represents the proportionality between shear stress and the difference in velocity across the lower boundary, i.e. $u(0) - 0$. For lower values of κ, the boundary slips more easily, whereas for higher values of κ, the boundary becomes stickier.

Upon solution the expression for velocity across the shear zone is given by:

$$u(y) = \frac{U(\kappa y + \mu)}{h\kappa + \mu} + \frac{G(h - y)(y\mu + h(\kappa y + \mu))}{2\mu(h\kappa + \mu)} \tag{2}$$

The velocity at the base of the shear zone is generally nonzero and is given by:

$$u(0) = \frac{Gh^2 + 2U\mu}{2(h\kappa + \mu)} \tag{3}$$

This shows that the higher the velocity (U) at the upper boundary, the higher the slip velocity at the lower boundary. However, no such simple statement can be made about the relationship between slip velocity and viscosity. Noting that $G > 0$ for movement up the channel, this expression is always positive. When the shear stress is zero along the base (i.e. $\kappa = 0$ perfect slip with $\lambda = \infty$), the basal velocity is:

$$u(0) = U + \frac{Gh^2}{2\mu} \tag{4}$$

Maximum velocity inside the shear zone will occur at one of the boundaries or inside the shear zone. Using standard analysis the location of the maximum occurs at:

$$y = \frac{\kappa\left(Gh^2 + 2U\mu\right)}{2G(h\kappa + \mu)} \tag{5}$$

This means that if $\kappa = 0$, then the maximum velocity occurs at the base of the shear zone as long as $G > 0$. In general the corresponding maximum velocity is:

$$u_{\max} = \frac{\left(2U\mu + Gh^2\right)\left(2\kappa^2 U\mu + G(h\kappa + 2\mu)^2\right)}{8G\mu(h\kappa + \mu)^2} \tag{6}$$

However, this maximum lies inside the shear zone (i.e. $0 \le y \le h$) only if:

$$G \ge \gamma_a = \frac{2\kappa U\mu}{h^2\kappa + 2h\mu} \tag{7}$$

along with $\kappa > 0$. This implies that the ductile shear sense is swapped inside the shear zone across the maximum. For example in Fig. 4a, the top two profiles have $G \ge \gamma_a$ and the shear sense changes from sinistral to dextral going from the lower to upper boundaries. In all other cases, the maximum velocity occurs at either the upper or lower boundary of the shear zone. Consequently, a single shear sense occurs throughout the shear zone. By comparing velocities at the two boundaries, the velocity at the base is greater than that at the top only if:

$$G > \gamma_b = \frac{2\kappa U}{h} \tag{8}$$

When $k > 0$, then $\gamma_b\gamma_a > 0$ allowing visualisation of typical expected velocity profiles (Fig. 4).

The velocity at the slipping boundary depends on many factors including μ, G, U, h and κ. In Fig. 4a $\kappa > 0$. The velocity profile with $G = 0$ is linear and increases from the lower to upper boundaries. This is similar to the velocity profile in a horizontal shear zone (green velocity profile in Fig. 2 of Mukherjee 2013) except that with slip there is a velocity discontinuity at the base. When $G > \gamma_a > 0$, the profile is quadratic and the maximum velocity is present at the upper no-slip boundary. However, when $G > \gamma_a$, the maximum velocity occurs inside the shear zone. If $G > \gamma_b$, then the velocity at the slipping base of the shear zone exceeds that at the upper no-slip boundary and the maximum velocity occurs inside the shear zone.

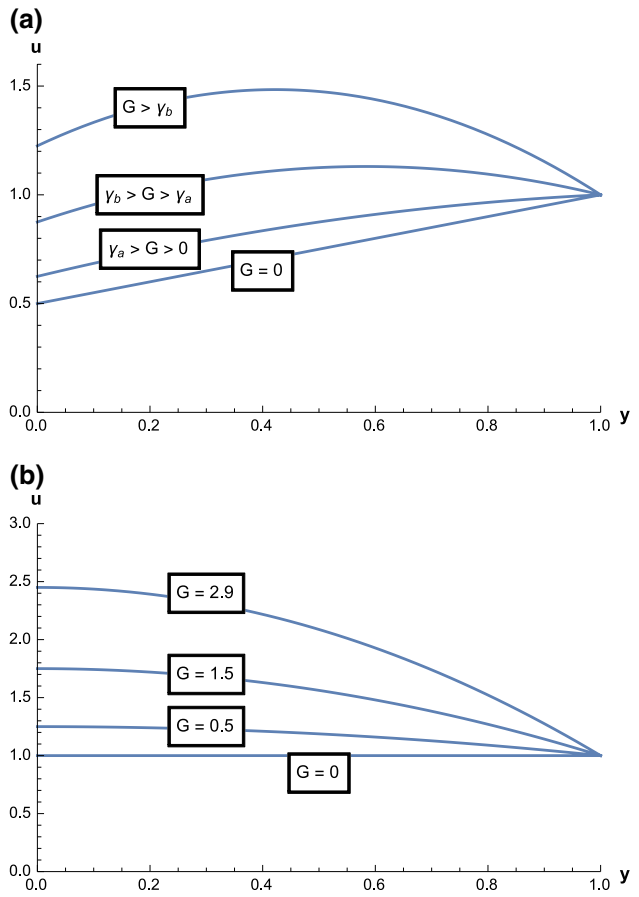

Fig. 4 Example velocity profiles with **a** $\kappa > 0, \gamma_a = \frac{2}{3}, \gamma_b = 2$ and **b** $\kappa = \gamma_a = \gamma_b = 0$

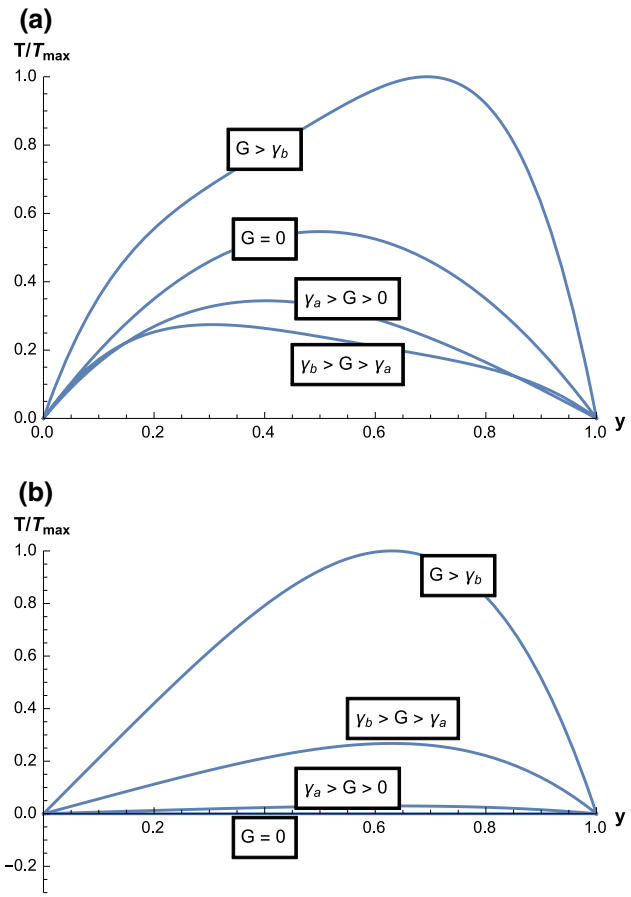

Fig. 5 Example temperature profiles corresponding to the parameters used in Fig. 4, with **a** $\kappa > 0, \gamma_a = \frac{2}{3}, \gamma_b = 2$ and **b** $\kappa = \gamma_a = \gamma_b = 0$. Temperature is scaled with the maximum temperature inside the shear zone ($T_{\max}$)

When the perfect slip condition is applied ($\kappa = 0$, see Fig. 4b), the maximum velocity always occurs at the lower slipping boundary, and velocity profiles are quadratic for $G > 0$. When $G = 0$, a plug-type flow, like that in Fig. 1c, is present. All material points inside the shear zone translate identically, and no shear sense develops. In this case, it is better not to call the zone a shear zone.

Temperature profiles

Following Turcotte and Schubert (2002), Lautrup (2011) and Mukherjee and Mulchrone (2013), the temperature (T) distribution inside the shear zone is governed by the following general equation:

$$k\frac{\mathrm{d}^2T}{\mathrm{d}y^2} + \mu\left(\frac{\mathrm{d}u}{\mathrm{d}y}\right)^2 = 0 \tag{9}$$

where k is thermal conductivity. Suitable boundary conditions are:

$$T(0) = T_\mathrm{l}, \quad T(h) = T_\mathrm{u}$$

where T_l and T_u are the temperatures at the lower and upper boundaries of the channel, respectively. The solution is:

$$T(y) = T_\mathrm{l} + \frac{(T_\mathrm{u} - T_\mathrm{l})y}{h} + \frac{U^2(h-y)y\kappa^2}{2k(h\kappa+\mu)^2} - \frac{GU(h-y)y\kappa(h(h-2y)\kappa - 2(h+y)\mu)}{6k\mu(h\kappa+\mu)^2} + \frac{G^2\left(h^2(h-y)y\left(h^2-2hy+2y^2\right)\kappa^2 + 4h(h-y)y^3\kappa\mu + 2y\left(h^3-y^3\right)\mu^2\right)}{24k\mu^2(h\kappa+\mu)^2} \tag{10}$$

Temperatures at the upper and lower boundaries are taken to be zero so that only the temperature due to shear heating (i.e. viscous dissipation) is shown. The temperature profile due to shear heating is illustrated in Fig. 5 for the parameters used in the velocity profile examples above. Asymmetrical temperature profiles occur for $G > 0$ (Fig. 5). For $G > \gamma_b$, the profile tends to attain it maximum near the upper boundary, whereas for $\gamma_b > G > 0$, the maximum is towards the lower boundary. If $G = 0$, parabolic

profiles symmetric about the shear zone centre are present. Interestingly, the same pattern of shear heat profile was deduced for no-slip boundary condition when $G = 0$ (Fig. 1 in Mukherjee and Mulchrone 2013). If in addition $\kappa > 0$, then the material translates with uniform velocity and no shear heating is present (Fig. 5b).

Applicability

The model developed applies to ductile simple shear zones whose behaviour can be approximated by a Newtonian fluid (Mulchrone and Mukherjee in press). Fortunately, sheared rocks with several chemical phases and minerals approximate as a single fluid in terms of deformation and flow behaviour, and this is especially true for oceanic crustal mafic rocks, lower continental crustal-hydrated mafic rocks and ophiolites (Hirth 2015). Secondly, the work remains valid so long that shear heating is insufficient to change the viscosity of the rock body (similar to Ramsay 1980; Mukherjee 2012 etc.). Thus, smaller the ductile shear zone, better would be the presented model. The perfect slip condition ($\kappa = 0$, $\lambda = \infty$) will not be present in natural materials including rocks. Therefore, Figs. 2b and 3b are not considered realistic models for flow in shear zones in rocks. Instead, the $\kappa > 0$ (partial-slip) cases shown in Figs. 2a and 3a are considered much more likely. The model presented can be extended for subduction channels (Mukherjee and Mulchrone 2013) and ductile simple shear zones where normal fault-like movement takes place possibly because an extrusive pressure gradient is not present (i.e. $G < 0$, Mukherjee 2014b). The shear zone was considered to be unaffected by metamorphism. As granitoids do not alter rheology due to metamorphism (Gerbi et al. 2015), the present work would fit more in ductile shear granitoids. Noting actual complicacy in ductile shear zones in prototype, Gerbi et al. (2015) rightly stated '… a simple algorithm predicting shear zone formation will not succeed in many geologically relevant instances'.

Acknowledgments S.M. thanks Department of Science and Technology (New Delhi) Young Scientist Project grant number: SR/FTP/ES/117/2009 for support. Christoph Schrank (Queensland University of Technology Brisbane) and Gretchen Baier (Dow Chemical Company) are thanked for reviewing. Editorial handling by Karel Schulman (Université de Strasbourg), Wolf-Christian Dullo (GeoMar) and Monika Dullo is acknowledged.

References

Beaumont C, Jamieson RA, Nguyen MH et al (2001) Himalayan tectonics explained by extrusion of a low-viscosity crustal channel coupled to focused surface denudation. Nature 414:738–742

Berthé D, Choukroune P, Jegouzo P (1979) Orthogneiss, mylonite and non-coaxial deformation of granites: the example from the South Armorican shear Zone. J Struct Geol 1:31–42

Bonaccurso E, Butt H-J, Craig VSJ (2003) Surface roughness and hydrodynamic boundary slip of a Newtonian fluid in a completely wetting system. Phys Rev Lett 90:144501

Boquet L, Barrat J-L (2007) Flow boundary conditions from nano- to micro-scales. Soft Matter 3:685–693

Boudier F, Al-Rajhi A (2014) Structural control on chromite deposits in ophiolites: the Oman case. In: Rollinson HR, Searle MP, Abbasi IA, Al Kindi MH (eds) Tectonic evolution of the Oman Mountains. Geol Soc, London, Spec Publ 392, pp 263–277

Czeck DM, Hudleston PJ (2004) Physical experiments of vertical transpression with localized nonvertical extrusion. J Struct Geol 26:573–581

Davis GH, Reynolds SJ, Kluth CF (2012) Structural geology of rocks and regions, 3rd edn. Wiley, New York

Duprat-Oualid S, Yamato P, Schmalholz SM (2015) A dimensional analysis to quantify the thermal budget around lithospheric-scale shear zones. Terra Nova 27:163–168

Eckert M (2006) The dawn of fluid mechanics: a discipline between science and technology. Wiley-VCH, New York, pp 1–175

Fleitout L, Froideavaux C (1980) Thermal and mechanical evolution of shear zones. J Struct Geol 2:159–164

Frehner M, Exner U, Mancktelow NS et al (2011) The not-so-simple effects of boundary conditions on models of simple shear. Geology 39:719–722

Gerbi C, Culshaw N, Shulman D, Foley M, Marsh J (2015) Predicting km-scale shear zone formation. Geophysical Research Abstracts, vol 17, EGU2015-3097, EGU General Assembly

Guo Z, Wilson M (2012) The Himalayan leucogranites: constraints on the nature of their crustal source region and geodynamic setting. Gondwana Res 22:360–376

Hirth G (2015) Application of flow laws to the rheology of shear zones. Geophysical Research Abstracts, vol 17, EGU2015-7117, EGU General Assembly

Hollister LS, Crawford ML (1986) Melt-enhanced deformation: a major tectonic process. Geology 14:558–561

Lauga E, Brenner MP, Stone HA (2007) Microfluids: the no slip boundary condition. In: Tropea C, Yarin AL, Foss JF (eds) Springer handbook of experimental fluid mechanics. Berlin, pp 1219–1240

Lautrup B (2011) Physics of continuous matter, 2nd edn. Taylor & Francis, London, p 381

Mukherjee S (2007) Geodynamics, deformation and mathematical analysis of metamorphic belts of the NW Himalaya. Unpublished Ph.D. thesis. Indian Institute of Technology Roorkee, pp. 1–267

Mukherjee S (2010) Structures in meso-and micro-scales in the Sutlej section of the Higher Himalayan Shear Zone, Indian Himalaya. e-Terra 7:1–27

Mukherjee S (2011) Mineral fish: their morphological classification, usefulness as shear sense indicators and genesis. Int J Earth Sci 100:1303–1314

Mukherjee S (2012) Simple shear is not so simple! Kinematics and shear senses in Newtonian viscous simple shear zones. Geol Mag 149:819–826

Mukherjee S (2013) Channel flow extrusion model to constrain dynamic viscosity and Prandtl number of the Higher Himalayan Shear Zone. Int J Earth Sci 102:1811–1835

Mukherjee S (2014a) Atlas of shear zone structures in meso-scale. Springer, Berlin

Mukherjee S (2014b) Kinematics of 'top -to-down' simple shear in a Newtonian rheology. J Ind Geophys Union 18:245–248

Mukherjee S (2015) Atlas of structural geology. Elsevier, Amsterdam

Mukherjee S, Koyi HA (2010) Higher Himalayan Shear Zone, Sutlej section: structural geology and extrusion mechanism by various

combinations of simple shear, pure shear and channel flow in shifting modes. Int J Earth Sci 99:1267–1303

Mukherjee S, Mulchrone KF (2013) Viscous dissipation pattern in incompressible Newtonian simple shear zones: an analytical model. Int J Earth Sci 102:1165–1170

Mukherjee S, Koyi HA, Talbot CJ (2012) Implications of channel flow analogue models for extrusion of the Higher Himalayan Shear Zone with special reference to the out-of sequence thrusting. Int J Earth Sci 101:253–272

Mulchrone KF, Mukherjee S (in press) Shear senses and viscous dissipation of layered ductile simple shear zones. Pure Appl Geophys. doi:10.1007/s00024-015-1035-8

Muntener O, Hermann J (2001) The role of lower crust and continental upper mantle during formation of non-volcanic passive margins: evidence from the Alps. In: Wilson RCL, Whitmarsh RB, Froitzheim N (eds) Non-volcanic passive margins: a comparison of evidence from Land and Sea. Geol Soc, London, Spec Publ 187, pp 267–288

Papanstasiou TC, Georgioi GC, Alexandrou AN (2000) Viscous fluid flow. CRC Press, Florida, pp 181–182, 198–203

Passchier CW, Trouw RAJ (2005) Microtectonics, 2nd edn. Springer, Berlin, p 116

Pozrikidis C (2009) Fluid dynamics: theory, computation, and numerical simulation, 2nd edn. Springer, New York

Ramsay JG (1980) Shear zone geometry: a review. J Struct Geol 2:83–99

Regenauer-Lieb K, Yuen DA (2003) Modeling shear zones in geological and planetary sciences: solid- and fluid-thermal–mechanical approaches. Earth Sci Rev 63:295–349

Richardson S (1973) On the no-slip boundary condition. J Fluid Mech 59:707–719

Rivers T (2009) The Grenville province as a large hot long-duration collisional orogen—insights from the spatial and thermal evolution of its orogenic fronts. In: Murphy JB, Keppie JD, Hynes AJ (Eds) Ancient orogens and modern analogues. Geol Soc, London, Spec Publ 327, pp 405–444

Schlichting H, Gersten K (1999) Boundary layer theory, 8th revised enlarged edition. Springer, Berlin

Turcotte D, Schubert G (2002) Geodynamics, 2nd edn. Cambridge University Press, Cambridge, p 284

Warren CJ, Beaumont C, Jamieson RA (2008a) Deep subduction and rapid exhumation: role of crustal strength and strain weakening in continental subduction and ultrahigh-pressure rock exhumation. Tectonics 27:TC6002

Warren CJ, Beaumont C, Jamieson R (2008b) Formation and exhumation of ultra-high-pressure rocks during continental collision: role of detachment in the subduction channel. Geochem Geophys Geosyst 9:Q04019

Warren CJ, Beaumont C, Jamieson RA (2008c) Modelling tectonic styles and ultra-high pressure (UHP) rock exhumation during the transition from oceanic subduction to continental collision. Earth Planet Sci Lett 267:129–145